Spectroscopy of autoionizing doubly excited states in ultracold Na_2 molecules produced by photoassociation

A. Amelink,[1] K. M. Jones,[2] P. D. Lett,[2] P. van der Straten,[1] and H. G. M. Heideman[1]
[1]*Debye Institute, Department of Atomic and Interface Physics, Utrecht University, P.O. Box 80 000, 3508 TA Utrecht, The Netherlands*
[2]*Atomic Physics Division, National Institute of Standards and Technology, Gaithersburg, Maryland 20899-8424*
(Received 27 October 1999; published 9 March 2000)

We have performed photoassociation spectroscopy to study the doubly excited states of Na_2 involved in the associative ionization of colliding Na($3P$) atoms. Rovibrational levels of two doubly excited potentials connected to the $P_{3/2}+P_{3/2}$ asymptote, one of 0_u^- and one of 1_u symmetry, have been identified. These two doubly excited potentials dominate the route to ionization used in photoassociation experiments of cold Na. Binding energies and rotational constants for all the vibrational levels with binding energies <50 GHz have been measured. The asymptotic potentials and short-range ionization probabilities are extracted from the data.

PACS number(s): 34.50.Gb

I. INTRODUCTION

The invention of methods for the laser cooling of atoms has enabled the development of high-resolution photoassociation spectroscopy of diatomic molecules [1–4]. Typically a sample of cold (≈ 1 mK) atoms is produced by laser cooling and held in a magneto-optical trap. A probe laser detuned red of the atomic resonance ($3S \rightarrow 3P$ for Na) is introduced and, when the laser frequency is properly chosen, two slowly colliding atoms absorb a photon to produce a molecule. One way to detect that photoassociation has occurred is to promote the molecules to an ionization continuum with a second photon and then detect the resulting positive ions. Spectroscopic information on molecular states connecting to the first excited molecular asymptote ($3S+3P$ for Na_2) can be obtained by scanning the first laser. From such spectra it has been possible to obtain information such as high precision molecular binding energies, atomic lifetimes, and ground-state scattering lengths [1].

Alternatively, one can fix the frequency of the first laser and use the photoassociation process to produce a sample of translationally cold molecules in a well defined rovibrational level. A second laser can be scanned to induce transitions to more highly excited molecular states [5,6]. In the case of doubly excited autoionizing states of Na_2 considered here, transitions can again be detected by monitoring the production of molecular ions. The photoassociation process favors production of molecules in long-range states; either high vibrational levels of deep, chemically bound potentials or vibrational levels of purely long-range potentials. These states generally have a good Franck-Condon overlap with high vibrational levels of more highly excited electronic potentials and thus are favorable intermediates for studying near-dissociation levels of doubly excited states. In the present experiment we use photoassociation to produce cold molecules in either of two intermediate states (0_g^- and 1_g at $3S+3P_{3/2}$) and produce spectra of autoionizing molecular states with binding energies less than 2 cm^{-1} below the $3P_{3/2}+3P_{3/2}$ asymptote. We find that two doubly excited molecular states dominate the ionization process from these intermediate states.

Figure 1 shows an ionization pathway used in previous photoassociation experiments on Na_2 [5,7,8]. Molecules produced by a photoassociation (PA) laser are dissociated by a second ''photoionizing'' laser (PI) into a pair of $3P$ atoms. Some of these pairs undergo associative ionization [$\mathrm{Na}(3P)+\mathrm{Na}(3P) \rightarrow \mathrm{Na}_2^+ + e^-$] at short range. In addition to the ionization pathway shown, the molecule may also be directly photoionized at short internuclear distances; however, the associative ionization pathway dominates once energetically permitted [8–10]. The second, ionizing step in Fig. 1 is a bound $\rightarrow$ free transition with relatively little structure on the scale of molecular linewidths. The behavior of the above-threshold ionization has been investigated [5], but the symmetries and properties of the doubly excited autoionizing states were not determined in that work. By studying the bound states just slightly below the $3P_{3/2}+3P_{3/2}$ disso-

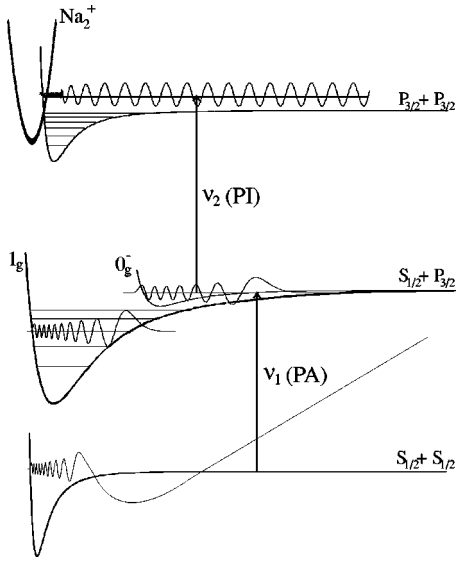

FIG. 1. An ionization pathway for detecting photoassociation of ultracold sodium. Two slowly colliding atoms absorb a photon (ν_1), detuned to the red of the atomic $3S \rightarrow 3P$ resonance, to produce a translationally cold singly excited molecule. A second photon (ν_2), blue of atomic resonance, promotes the molecule to an unbound autoionizing state.

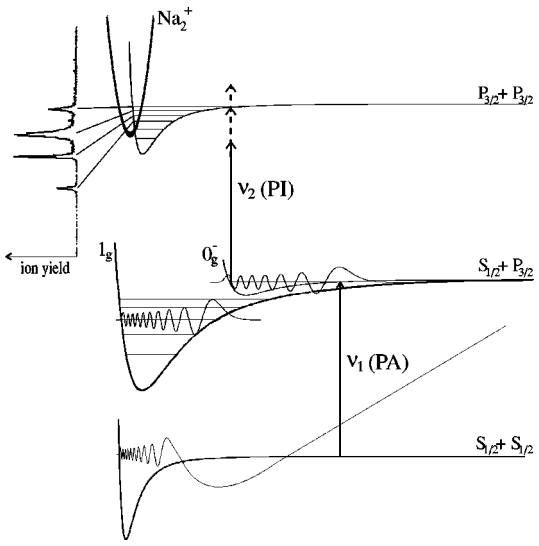

FIG. 2. Schematic diagram of the experiment. The PA laser (red detuned) is fixed on a rovibrational level of either the singly excited 1_g or 0_g^- potential [Hund's case (c) notation], while the PI laser (blue detuned) is scanned through the doubly excited $P_{3/2}+P_{3/2}$ asymptote. Ion peaks arising below this asymptote are due to excitation of bound doubly excited states.

ciation limit we can identify the molecular symmetry of the states involved and from the linewidths infer the autoionization rates. The question of the identity and properties of the autoionizing molecular states connected to the Na_2 $(3P+3P)$ asymptote naturally arises in the study of associative ionization in thermal collisions of $Na(3P)$ atoms as well [11–13]. In this case collisions occur on doubly excited molecular potentials of any symmetry whereas in our case, by choosing the symmetry of the intermediate state, doubly excited molecular potentials of specific symmetries can be studied separately. Our results provide important tests for quantum chemistry calculations [12,13] which seek to model the thermal associative ionization process. Reproducing our results does not require averaging over thermal distributions and molecular symmetries and thus permits a more detailed and direct test of the calculations.

II. EXPERIMENT

The experiments are performed in a ''dark spot'' magneto-optical trap [14] which leaves almost all the atoms in the lowest, $f=1$, hyperfine level of the $3S_{1/2}$ ground state. The trap is continuously loaded from a Zeeman-tuned, laser cooled atomic beam [15]. The trapping beams are turned on and off at a 100 kHz rate with a duty cycle of 50%. During the trap-off periods two probe beams are superimposed and focused into the region with the highest density of trapped atoms. The two beams have orthogonal polarizations and are combined using a polarizing beamsplitter cube. Low powers are used in order to avoid power broadening and skewed line shapes [5]. Molecular ions created during the probe periods are collected and counted with a channel electron multiplier.

To study the doubly excited states of Na_2 involved in the ionization process, the experiment shown schematically in Fig. 2 is performed. The frequency of the PA laser is detuned to the red of the atomic $3S_{1/2}\rightarrow 3P_{3/2}$ resonance while the PI laser is detuned to the blue. The frequency of the PA laser is chosen to drive a transition from colliding ground-state atoms to a specific rovibrational level of the 1_g or 0_g^- potential. The frequency of the PI laser is scanned to drive transitions from the chosen intermediate state to levels up to and above the $P_{3/2}+P_{3/2}$ threshold. Peaks in the ion spectrum below this threshold correspond to bound levels of the doubly excited potentials.

The frequency tuning of the PA laser was determined for the 0_g^- rovibrational levels in previous experiments [7]. The detuning of the PI laser is determined using frequency markers from a calibrated 300 MHz free spectral range confocal étalon, locked to an atomic transition. This allows us to determine the binding energies of levels in the doubly excited potential to approximately 20 MHz. For spectra taken when the PA laser is tuned onto a 1_g level, the binding energies are not as accurately known as for the 0_g^- states. In this case the étalon is used to generate a linear frequency scale for the PI laser and the zero of the scale is determined by matching strong features in these spectra to ones that also appear in the spectra taken with the 0_g^- intermediate states.

III. RESULTS

A. Spectroscopic data

The energies and rotational constants of the low vibrational levels of the singly excited 0_g^- potential have been accurately determined elsewhere [7]. The rotational spacing is found to be large enough to resolve most of the rotational structure, which enables us to fix the PA laser frequency on each rovibrational level separately. This is crucial for the determination of the symmetries of the doubly excited states involved in the ionization process, as discussed below.

In Fig. 3 the PA laser frequency is fixed on different rotational levels of the $v=0$ and $v=1$ states of the 0_g^- potential. Since the $J=0$ rotational level is not completely resolved from the $J=1$ level, we fixed the PA laser on the $J=0$ rotational level in the $v=0$ state [Fig. 3(a)]. In this vibrational state the $J=1$ rotational level is nearly absent due to a node in the *p*-wave ground-state wave function [16]. This minimizes the contributions from $J=1$ in the $J=0$ ion spectrum. The $J=1$ rotational level is also not completely resolvable from the $J=2$ feature; a small amount of the $J=2$ spectrum is therefore subtracted from the $J=1$ spectrum in the figure to correct for this. We have also fixed the PA laser on rotational levels of the $v=5$ and $v=6$ vibrational states, yielding similar results.

The spectra in Fig. 3 consist of ion peaks below the $3^2P_{3/2}(f=3)+3^2P_{3/2}(f=3)$ threshold, corresponding to bound doubly excited states, and a Condon internal diffraction pattern above this asymptote as reported previously [5]. Our focus is on the bound states, which contain information about the potentials involved in the ionization process. Excitation from the intermediate 0_g^- state is restricted to doubly excited Hund's case (c) states of 0_u^- and 1_u symmetry. For excitation to a 1_u state the usual electric dipole selection rule

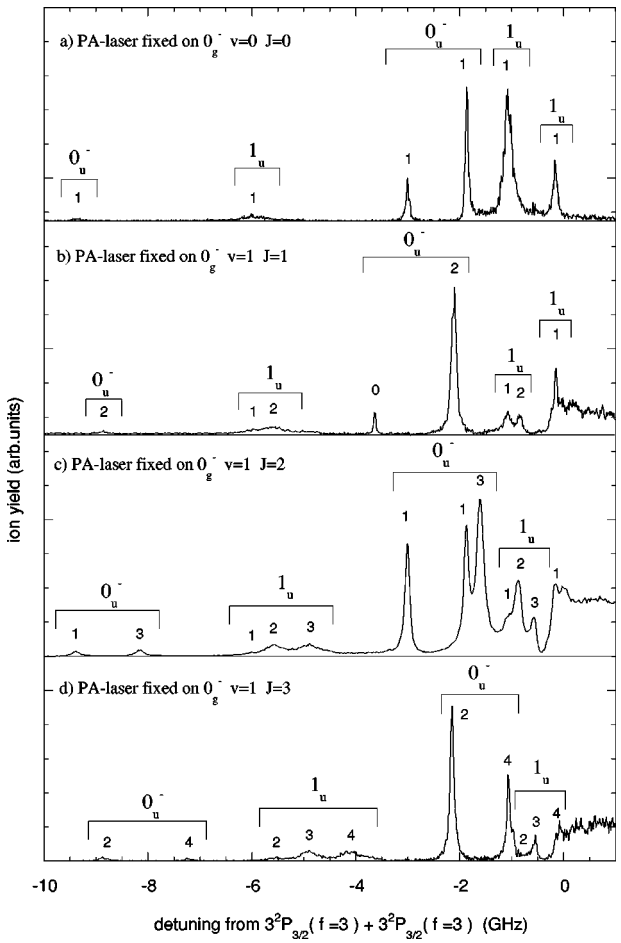

FIG. 3. Measurement with the PA laser fixed on the $0_g^-(v=0$ and 1) vibrational levels. From top to bottom the rotational quantum numbers are $J=0$, 1, 2, and 3, respectively. Changing v has very little effect on the spectra. The numbers displayed are the rotational quantum numbers J' of the doubly excited states. Identification of the peaks is based on selection rules, as explained in the text.

$\Delta J=0,\pm 1$ holds. For excitation to a 0_u^- state the Q branch $(\Delta J=0)$ transition is forbidden [17]. These selection rules permit us to identify both the molecular symmetry and the rotational quantum number of the observed doubly excited rovibrational levels.

In Fig. 3 we have identified two vibrational levels of each molecular symmetry 0_u^- and 1_u, as indicated. For the vibrational levels labeled 0_u^- the Q branch is clearly missing. Figure 4 shows that the lines fit well to rotational progressions. The rovibrational levels of the 0_u^- state do not follow the straight lines as closely as for the 1_u state. In addition, the highest vibrational level of the 0_u^- state has two candidate $J'=1$ features, which lie equidistant from a line fitted to fthe higher rotational features, suggesting an accidental degeneracy with a level from another state.

It is observed that the widths of the ion peaks depend on the vibrational quantum number and the symmetry of the molecule, but not on the rotation, as explained in Sec. III C. The peak heights of the highest rovibrational levels (nearest to dissociation) are an order of magnitude larger than the

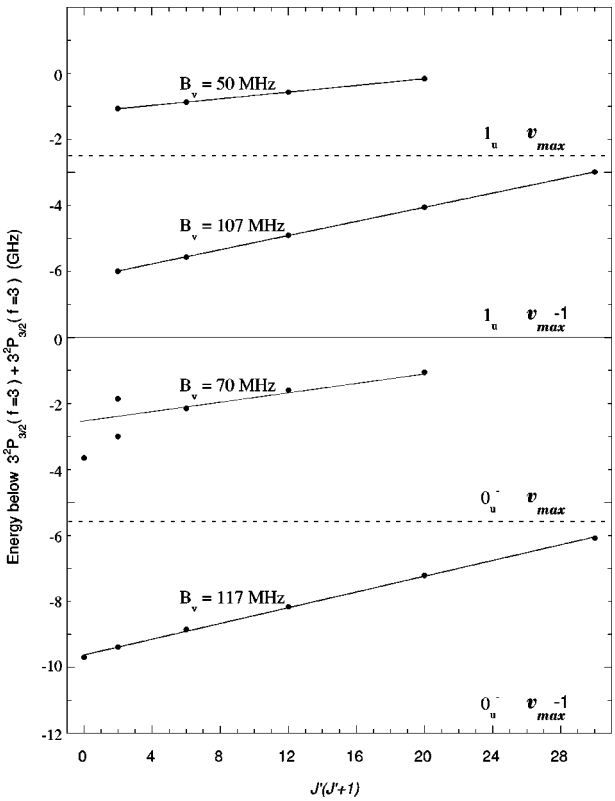

FIG. 4. Rotational progressions of the least bound states of the doubly excited 1_u and 0_u^- potentials. The slopes of the straight lines are equal to the rotational constants B_v.

lower ones, and no additional bound states have been observed for red detunings larger than 10 GHz with the PA laser fixed on a 0_g^- rovibrational level. This is due to the fact that the outer turning points of more deeply bound doubly excited vibrational levels are at an internuclear distance which is too small to have any substantial overlap with the 0_g^- vibrational levels. This is shown schematically in Fig. 2. The singly excited 0_g^- state is a purely long-range state with an inner turning point of $\approx 55a_0$. It will be shown that the asymptotic potential for both of the observed doubly excited states is consistent with a C_5/R^5 interaction, with $C_5 \approx -250$ a.u. (cf. Sec. III B). (The atomic units for C_5 are hartree$\times a_0^5$, where 1 hartree$=4.359\times 10^{-18}$ J, and $1a_0 = 0.5292\times 10^{-10}$ m.) The outer turning point of a doubly excited vibrational level with a binding energy E is easily estimated by $R_{outer}=(C_5/E)^{1/5}$, and for vibrational levels bound by more than 10 GHz the outer turning point is calculated to be less than $44a_0$. Consequently, the overlap of these levels with the intermediate 0_g^- vibrational levels vanishes.

To observe more deeply bound rovibrational levels we fixed the PA laser on the 1_g $(v=63)$ level. This level is bound by ≈ 720 GHz and has an outer turning point of $\approx 41a_0$ and therefore has a better Franck-Condon overlap with the lower vibrational levels of the doubly excited potential than any of the 0_g^- levels do. Figure 5 shows spectra recorded with the PA laser fixed on the 1_g $(v=63, J=1, 2, 3,$ and 4) rotational levels. As expected, additional

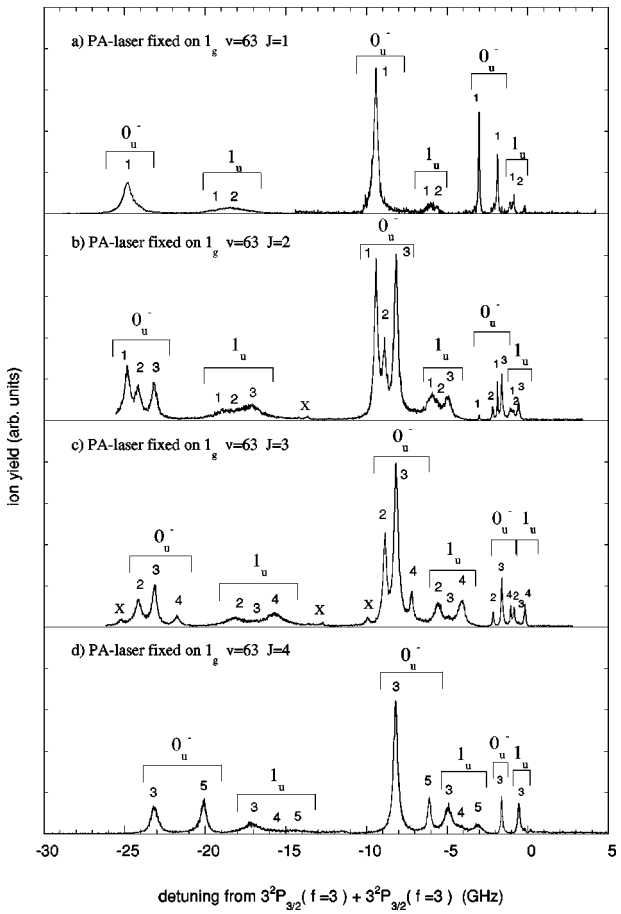

FIG. 5. Measurement with the PA laser fixed on the 1_g ($v=63$, $J=1$, 2, 3, and 4) states. This vibrational state has an outer turning point at $41a_0$. Fixing the PA laser on different vibrational levels changes the outer turning point and thus the overlap with the doubly excited states. This is observed as a change in the relative population of the three vibrational levels of the 0_u^- and 1_u potentials. The X's indicate unidentified lines, possibly from a 2_u potential.

rovibrational levels are observed at red detunings larger than 10 GHz. The ion peak widths and peak positions of the levels observed at detunings smaller than 10 GHz in Fig. 5 are identical to those of Fig. 3. The peak heights are different due to a different wave function overlap. The small structures of Fig. 3 are reproduced as the largest structures in Fig. 5, and the small structures of Fig. 5 near dissociation are identical to the large structures in Fig. 3. The identification of the vibrational levels below -10 GHz is based on their relative widths and relative peak heights. We have observed similar spectra using the $v=60$, $v=65$, and $v=67$ levels of the 1_g potential as the intermediate step. In addition to the states shown, another level of the 0_u^- state (off-scale in Fig. 5) is observed near -50 GHz with the PA laser fixed on the $v=60$ level. This signal is small compared to the others, possibly due to a small wave function overlap with the 1_g ($v=60$) rotational states. The uncertainty in the binding energies of these rovibrational levels is somewhat larger (≈ 0.2 GHz, see Table I).

TABLE I. Spectroscopic data of the doubly excited 0_u^- state asymptotically connected to $P_{3/2}+P_{3/2}$. Displayed are the binding energies E_{vJ} of the rovibrational levels in GHz relative to the $P_{3/2}(f=3)+P_{3/2}(f=3)$ asymptote. The highest vibrational level ($v=v_{max}$) contains both values for $J=1$ (see also Fig. 3 and Fig. 4). The rotational constants for the lowest vibrational levels are $B_{v_{max}-3}=230$ MHz and $B_{v_{max}-2}=170$ MHz. Estimated statistical uncertainties given here, and elsewhere in this paper, are one standard deviation uncertainties.

J	v_{max}-3	v_{max}-2	v_{max}-1	v_{max}
0		$-25.16(2)$	$-9.69(2)$	$-3.67(2)$
1	$-51.5(2)$	$-24.84(2)$	$-9.38(2)$	$-3.00(2); -1.86(2)$
2	$-50.6(2)$	$-24.15(2)$	$-8.85(2)$	$-2.15(2)$
3	$-49.2(2)$	$-23.15(2)$	$-8.16(2)$	$-1.60(2)$
4	$-47.4(2)$	$-21.74(2)$	$-7.21(2)$	$-1.06(2)$
5		$-20.10(2)$	$-6.08(2)$	

In Fig. 5 the $J'=4$ states are missing in the 0_u^- vibrational levels with the PA laser fixed on the $J=4$ level, whereas the 0_u^- ($J'=1$) states are the only ones present with the PA laser fixed on the $J=1$ state. In fact, we were able to make either the Q branch or the P and R branches of the 0_u^- states disappear completely by shifting the PA laser frequency by less than the width of the 1_g rotational line. In the singly excited 1_g potential every rotational level J has both odd and even I hyperfine components which are partially resolved. In the doubly excited 0_u^- state even (odd) J' have only even (odd) I', as discussed in the Appendix. By tuning the PA laser slightly we excite different hyperfine levels of the 1_g state, i.e., levels with the same J but different I. Since the nuclear spin is not changed in an electric dipole transition this causes the disappearance of either the odd or even rotational levels of the 0_u^- state, depending on whether the PA laser was fixed on a hyperfine level with even or odd nuclear spin, respectively. To observe both odd and even doubly excited rotational levels at the same time [see Figs. 5(b) and 5(c)], the power of the PA laser can be increased so that multiple hyperfine levels of the 1_g potential are excited simultaneously.

A list of all the binding energies of the doubly excited 0_u^- and 1_u rovibrational levels is given in Tables I and II, respectively. Apart from the states we identified in Fig. 5 as belonging to either the 0_u^- or 1_u potentials, other states are

TABLE II. Spectroscopic data of the doubly excited 1_u state asymptotically connected to $P_{3/2}+P_{3/2}$. Displayed are the binding energies of the rovibrational levels in GHz. The rotational constant for the lowest vibrational level is $B_{v_{max}-2}=175$ MHz.

J	v_{max}-2	v_{max}-1	v_{max}
1	$-18.85(2)$	$-5.99(2)$	$-1.07(2)$
2	$-18.16(2)$	$-5.56(2)$	$-0.87(2)$
3	$-17.13(2)$	$-4.91(2)$	$-0.57(2)$
4	$-15.70(2)$	$-4.05(2)$	$-0.16(2)$
5	$-14.2(5)$	$-2.99(2)$	

observed, which we have labeled X in the figure. Electronic transitions from the singly excited 1_g state can be made to the doubly excited 0_u^-, 0_u^+, 1_u, and 2_u states in Na_2. Our Movre-Pichler analysis (cf. Sec. III B 1) shows that only the 0_u^-, 1_u, and 2_u states that connect to the $P_{3/2}+P_{3/2}$ asymptote are attractive. The states labeled X can therefore possibly be assigned to the 2_u state; another possible explanation is that they are perturbations from other states.

B. Determination of the asymptotic potentials

Vibrational spectra can be used to extract the interaction potential for a particular state. As is well known, the energies of the least-bound vibrational states are principally determined by the long-range behavior of the potential. The leading term in the inverse power expansion for the long-range force between two Na($3P$) atoms is the electrostatic quadrupole-quadrupole interaction resulting in a potential which goes as C_5/R^5. The magnitude of the C_5 coefficient depends on the relative orientation of the two $3P$ atoms, i.e., on the symmetry of the molecular state. Marinescu [18] has published C_5 coefficients as well as higher order dispersion coefficients, C_6 and C_8, for the $3P+3P$ asymptote. His calculation does not take into account the fine structure of the atomic states, however. Since we are probing states connected asymptotically to the $3P_{3/2}+3P_{3/2}$ asymptote, and since the fine-structure splitting is much larger than the binding energy of the states detected, it is essential to include fine structure in the analysis.

1. Movre-Pichler analysis at long range

Movre and Pichler (MP) [19] have developed a model for molecular states connected to the $3S+3P$ limit which includes the combined effects of long-range forces and the atomic fine-structure splitting. This model has been very helpful in understanding the molecular states connected to this asymptote (see, for example, Ref. [7]). The underlying assumption of the MP model is that the molecular states can be fully described as combinations of $3S$ and $3P$ atomic orbitals centered on the two atomic cores. Heather and Julienne (HJ) have carried out a similar analysis for molecular states connecting to the $3P+3P$ asymptote [20]. They found that the MP model predicted a 1_u state which would be a shallow, purely long-range state with an inner turning point at $(20–25)a_0$ (and thus would not be autoionizing). The 0_u^- state, which we now know to also be important, was not discussed because it was predicted to be even shallower than the 1_u state. These calculations led them to conclude that a MP type model was not sufficient to understand the autoionizing states. Subsequently, Marinescu has improved the calculations of C_5 and C_6 coefficients and, in addition, calculated C_8 coefficients which were not included in the HJ analysis. Marinescu's C_5 coefficients are generally about 4.5% higher than those used by HJ, but for the Σ states involved here they are significantly different.

We have repeated the MP calculations using the new C_5's (but not including C_6 or C_8 terms). We find that the 1_u state of interest is still a shallow ($\approx$10 GHz), purely long-range state with inner turning points near $22a_0$. In addition to the 1_u state we also find that there is a state of 0_u^- symmetry that is attractive and connected to the $P_{3/2}+P_{3/2}$ asymptote; this difference from the HJ analysis is due to using Marinescu's revised C_5's for the Σ states. It remains an open question whether inclusion of C_6 and C_8 terms in the MP model will adjust the 1_u and 0_u^- potentials to be deep enough to reproduce our observations of autoionizing levels bound by 19 and 51 GHz.

Given the success of the MP-type calculation for molecular states at $3S+3P$, this failure to produce realistic potentials near $3P+3P$ would be an indication that it is necessary to include other atomic orbitals besides the $3P$. This is quite plausible since the $3P+3P$ asymptote is much closer to other, higher asymptotes than is the $3S+3P$ asymptote. Quantum chemistry calculations [21] have concluded that avoided crossings with states from other asymptotes at about $25a_0$ can significantly perturb the molecular potentials in the range relevant to our experiments. Data such as ours should help assess the accuracy of such *ab initio* calculations.

Despite the uncertainty about how well the MP model works over the whole distance range relevant to our experiment, we expect that the long-range behavior should be correct and we will use it to estimate the C_5 coefficient at long range. The MP model predicts that as $R\rightarrow\infty$ the 0_u^- state we observe is a mixture of a $^3\Pi_u$, $^1\Sigma_u^-$, $^3\Sigma_u^+(a)$, and $^3\Sigma_u^+(b)$ state. [The labels (a,b) refer to Eq. (3.14,15) of Ref. [18].] The mixture is in the proportion 6:12:8:1 and the C_5 coefficients for these states are -1526, 0, 0, and 2289, respectively, in atomic units. The resulting mixture has $C_5(0_u^-)=-254.4$ a.u. At an internuclear distance of $60a_0$ the effective C_5 value deviates only $\approx$10% from its asymptotic value. The 1_u state is a mixture of $^3\Sigma_u^+(a)$, $^3\Sigma_u^+(b)$, $^3\Pi_u$, and $^1\Pi_u$ states in the proportion 2:1:3:3, respectively, and has the same C_5 as the 0_u^- state. Strictly speaking, before comparing this potential to an experimentally derived rotationless $(J=0)$ potential one should correct the theoretical potential to include the mechanical rotational energy of the $J=0$ level (see, for example, Ref. [7]). Given that we are using the MP model largely to suggest the form of the long-range potential, we have not tried to include what we expect to be a minor correction.

2. Accumulated phase method

Our previous discussion has shown that we expect that the potentials for both of the states that we have observed should be C_5/R^5 at long range, but may deviate from this even for the highest few bound states. Guided by this result we start by trying to fit our data to a C_5/R^5 potential. For this purpose we have used the accumulated phase method [22–24]. In this analysis it is assumed that the phase ϕ^{in} of the wave function for a bound state at a distance R_0 is nearly independent of the particular vibrational state chosen. For this approach to be useful R_0 must be at a sufficiently long range that the potential is given by its long-range form, yet also be at short enough range that the potential at R_0 is much deeper than any of the vibrational levels under consideration.

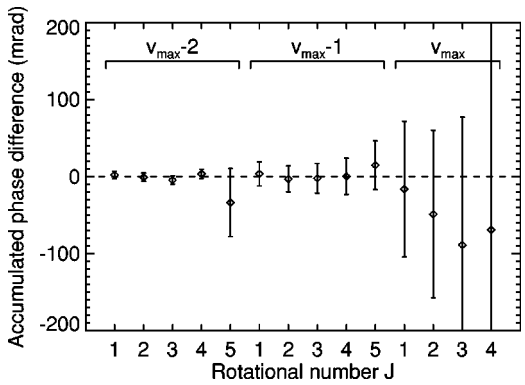

FIG. 6. Residuals for the best fit of the spectroscopic data of the 1_u state.

For a given long-range potential $V(R)$ and an experimentally determined rovibrational binding energy E_{vJ}, the asymptotic wave function can be calculated by numerical solution of the Schrödinger equation at large R:

$$\left[-\frac{\hbar^2}{2\mu}\frac{d^2}{dR^2}+V(R)+\frac{\hbar^2 J(J+1)}{2\mu R^2}\right]\psi(R)=E_{vJ}\psi(R), \quad (1)$$

with μ the reduced mass of the molecule. The potential $V(R)$ is the rotationless $(J=0)$ potential. For the integration we employ the standard Numerov method where the logarithmic derivative (ψ'/ψ) is determined by integrating from long range up to R_0. The phase ϕ^{out} is then determined using the relation $(\psi'/\psi)=k\,\text{cotan}(\phi^{\text{out}})$ with k the local wave vector. For a bound state the logarithmic derivative at R_0 calculated by integrating out from the inner region must equal that calculated by integrating in from the outer region, and thus the phase ϕ^{in} must equal the phase ϕ^{out} (mod π).

The phases ϕ^{out}_{vJE} of the rovibrational wave functions are then fitted to

$$\phi^{\text{out}}_{vJE}=\phi^{\text{in}}_0+\alpha J(J+1)+\beta E_{vJ} \quad (\text{mod } \pi) \qquad (2)$$

with ϕ^{in}_0, α, and β constants. The terms in α and β correct for the small dependence of the phase ϕ^{in} on rotation J and energy E_{vJ}. (Note that we have dropped the primes in the labeling of the quantum numbers of the doubly excited states.) For the long-range potential $V(R)$ we initially consider a pure C_5/R^5 potential since the MP calculations tell us that this is the leading term asymptotically. The value of C_5 is adjusted until the sum of the squares of the residuals of the fit to Eq. (2) is minimized. The points were weighted as explained below.

Figure 6 shows the residuals between the phases ϕ^{out}_{vJE} calculated for each level by solving the Schrödinger equation and those calculated from Eq. (2). Here, as elsewhere in this paper, the error bars indicate our estimate of a one standard deviation uncertainty. The phase ϕ^{out}_{vJE} changes by π going from one vibrational level to the next. Therefore the uncertainty in the phase is approximately given by $\pi/\Delta E$ times the experimental uncertainty in the binding energy, where ΔE is the splitting between the vibrational levels. Since ΔE becomes small close to the dissociation limit, the uncertainty in the phase increases with vibrational number.

We find that $C_5=-232(6)$ a.u. for the 0^-_u state and $C_5=-267(30)$ a.u. for the 1_u state, which is close to the theoretical asymptotic value -254.4 a.u. (discussed in Sec. III B 1). The fit reproduces the data within the estimated uncertainties. We have checked that the fitting procedure is independent of our choice of R_0 by choosing values of R_0 between $10a_0$ and $20a_0$. The nodes of the asymptotic wave functions calculated for different choices of R_0 do not change by more than $0.1a_0$ and the variation in C_5 is less than the standard deviation.

The error bar on C_5 represents only the statistical uncertainty and not the systematic uncertainty about the appropriateness of using a purely $1/R^5$ potential. As has been noted before [25], statistical error bars from a fit to a single model can greatly underestimate the actual uncertainty in a long-range parameter when the form of the potential is not known. To explore this further we have also fit the data to a purely $1/R^6$ potential. The quality of the fit is also good but gives a C_6 coefficient about five times larger than any value predicted by Marinescu [18]. The outer turning points resulting from this fit lie at such large internuclear distances that the state would have to be very shallow to reproduce the observed rotational constants. Furthermore, the outer turning points of the levels in this C_6/R^6 potential lie at larger internuclear distances than the outer turning points in the C_5/R^5 potential and thus, in the spectrum using the 0^-_g state as the intermediate state, one would expect to see more vibrational levels than just the two that we observe (Fig. 3). Thus we expect that the pure C_5/R^5 potential is a better approximation than the pure C_6/R^6 form. We cannot, however, rule out that adding a C_6/R^6 term, or even higher order terms, to the C_5/R^5 potential might change the C_5 coefficients mentioned above by more than their statistical error bars.

Although the question is not entirely settled, it seems that the Movre-Pichler model discussed in Sec. III B 1 predicts doubly excited potentials that deviate strongly from the pure C_5/R^5 behavior over the distance ranges relevant for even the highest few bound states of the potentials. Given that our data is well described by a potential which is C_5/R^5, or at least dominantly so, the indications are that a complete understanding of the potentials will require consideration of mixing with potentials from other atomic asymptotes. Given a calculated potential, finding bound states is a straightforward process and a direct comparison to the data (Tables I and II) is likely to be more fruitful than comparison with extracted dispersion coefficients such as C_5.

The calculated asymptotic wave functions of the least-bound 1_u vibrational levels, assuming that a pure $1/R^5$ potential is correct, are plotted in Fig. 7 along with the $v=1$ vibrational wave function of the singly excited 0^-_g potential. This figure clearly shows that only the highest two bound states have reasonable Franck-Condon overlap with the 0^-_g $(v=1)$ level, whereas the outer turning point of the third vibrational level is at too small an internuclear distance to have any noticeable overlap with this 0^-_g state, in agreement with our observations.

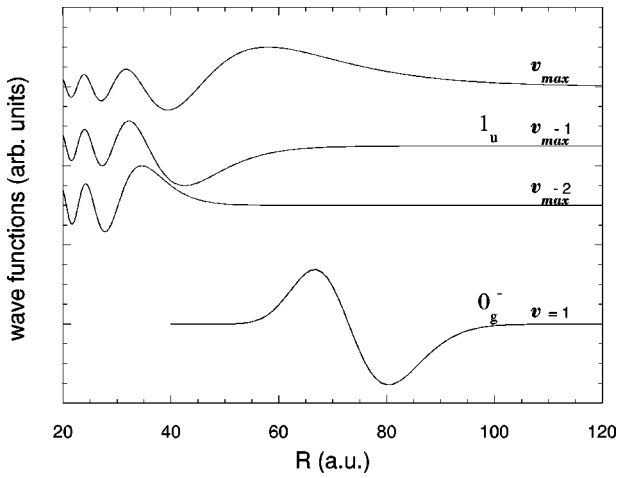

FIG. 7. Wave functions of the three least-bound vibrational levels of the doubly excited 1_u potential, along with the wave function of the $v=1$ vibrational level of the singly excited 0_g^- potential. Clearly the overlap of the 0_g^- wave function with the 1_u wave functions decreases rapidly with decreasing 1_u vibrational level. The (relative) Franck-Condon factors are 1.0, 0.26, and 3×10^{-3} for these three overlap integrals.

In addition to the value of C_5 the fit returns values for α, β, and $\phi_0^{\rm in}$. For example, for the 1_u potential and with $R_0=12a_0$, we find $\alpha=3.1$ mrad, $\beta=-16.9$ mrad/GHz, and $\phi_0^{\rm in}=-5.186$ rad. One can relate these parameters to the positions of the nodes of the wave functions. The nodal positions depend on the inner part of the potential as well as on the asymptotic part, and therefore contain additional information about the doubly excited potentials. Although the asymptotic potentials of the 0_u^- and 1_u states are nearly identical, the node positions of their least-bound wave functions are different. This difference in nodal positions can be expressed in terms of a ''scattering length'' (recognizing that for a short-lived excited state the connection between this parameter and the low-energy scattering properties is not as simple as for a long-lived ground state).

In the inner region of the potential the wave function of an unbound state with very small kinetic energy closely resembles the wave function of the least-bound states. It is therefore possible to calculate the scattering length a_s by numerically integrating the Schrödinger Eq. (1) for very small positive E, using the phase $\phi_0^{\rm in}$, α, and β determined from the bound states. We find $a_s=-44$ and 125 a_0 for the 0_u^- and 1_u potentials, respectively.

C. Ionization probabilities

It is also possible to extract ionization probabilities from the widths of the spectral lines. If the ion peaks belonging to each state are compared (Fig. 3 and Fig. 5), it can be seen that the widths Γ_{ion} of the ion peaks of the 1_u states are larger than those of the 0_u^- states. Furthermore, the widths decrease with increasing vibrational quantum number for both states. Using a semiclassical model we can interpret the linewidths in terms of an ionization probability per vibrational oscillation. The bound doubly excited molecules vibrate between their classical inner and outer turning points. Autoionization may occur each time the molecules are in the vicinity of the inner turning point, with a certain probability P_{ion}. For each vibrational level we calculate the number of oscillations before autoionization occurs $N_{osc}=\nu_{osc}\tau$ where the lifetime $\tau=1/\Gamma_{ion}$, and ν_{osc} is the local oscillator frequency approximated by $h\nu_{osc}=dE/dv$. The values for ν_{osc}, $\Gamma_{ion}/2\pi$, and N_{osc} are given in Table III. Note that the widths of the ion peaks $\Gamma_{ion}/2\pi$ are much larger than the atomic natural linewidth ($\Gamma_{at}/2\pi=10$ MHz), indicating that the decay of the doubly excited molecules is much faster than the natural radiative lifetime. The numbers quoted for Γ_{ion} are averaged over all of the data; the uncertainty is approximately 20%. For both states we observe that N_{osc} is approximately constant with the vibrational number. This implies that the probability of the ionization is independent of vibrational level. The ionization probability P_{ion} for each vibration is determined from the relation $(1-P_{ion})^{N_{osc}}=1/e$. We find that for the 1_u state $P_{ion}=34\%$ and that for the 0_u^- state $P_{ion}=15\%$. This analysis assumes that ionization is the only loss mechanism and thus represents an upper bound on the ionization probability.

TABLE III. Peak widths and local oscillator frequencies for all observed vibrational states. The peak widths are independent of the rotational quantum number J. The local oscillator frequency is calculated for the $J=2$ rotational states; the values for the other rotational levels are close to this value.

State	v	$\Gamma_{v,ion}/2\pi$ (MHz)	ν_{osc} (GHz)	N_{osc}
0_u^-	v_{max}	117	4.1	5.6
	v_{max}-1	285	10.7	6.0
	v_{max}-2	5×10^2	20.8	6.6
	v_{max}-3	8×10^2	31.8	6.3
1_u	v_{max}	160	2.2	2.2
	v_{max}-1	470	7.8	2.6
	v_{max}-2	1230	18.2	2.4

IV. CONCLUSION

We have measured and identified rovibrational levels of doubly excited 0_u^- and 1_u potentials near the $3P_{3/2}+3P_{3/2}$ asymptote. These potentials play a dominant role in the ionization pathway used in previous two-color photoassociation spectroscopy experiments. Excitation from the 0_g^- intermediate state occurs from the inner turning points of its vibrational levels to the outer turning points of the doubly excited bound states; as a result only the highest two doubly excited vibrational levels are accessible from the 0_g^- potential. In contrast, excitation from the 1_g intermediate states occurs primarily from the outer turning points of its vibrational levels. Consequently, lower doubly excited vibrational levels are observable starting from deeply bound 1_g vibrational levels. This spectroscopic data provides constraints on quantum chemistry calculations of the molecular potentials important for associative ionization of thermal Na($3P$) atoms. The states observed in the present experiments will certainly be

among the open channels in those experiments, although other channels may contribute to the ionization as well.

ACKNOWLEDGMENTS

This work is part of the research program of the ''Stichting voor Fundamenteel Onderzoek der Materie'' (FOM), which is financially supported by the ''Nederlandse Organisatie voor Wetenschappelijk Onderzoek'' (NWO). This work was supported by NIST and the U.S. Office of Naval Research. We thank G. C. Hill for contributions to the data acquisition and analysis.

APPENDIX: THE RELATION BETWEEN J AND I FOR HUND'S CASE (C) $\Omega=0$ STATES

The connection between the total nuclear spin I and the rotational quantum number J in a homonuclear diatomic molecule has been discussed before (see, for example, the discussion of ortho and parahydrogen in Ref. [17]). In this Appendix we will discuss the argument needed to derive the connection between I and J for states where the angular momentum coupling is Hund's case (c) rather than case (a).

The underlying physical principle that produces a connection between J and I in a homonuclear diatomic molecule is the requirement that the total molecular wave function must be symmetric (antisymmetric) under exchange of the identical nuclei when the individual nuclei are bosons (fermions). In the approximation that J (the angular momentum exclusive of nuclear spin) is a good quantum number, the wave function can be written as a product of a molecular part and a nuclear spin part in which the two atomic nuclear spins $i_{a,b}$ are coupled to produce a total spin I:

$$|\psi_{total}\rangle = |\psi_{mol}\rangle |(i_a i_b) I\rangle. \tag{A1}$$

For fermionic nuclei (such as ^{23}Na where $i_a = i_b = 3/2$) the behavior of the nuclear spin part of the wave function under exchange of the nuclei P is

$$P|(i_a i_b) I\rangle = (-1)^{I+1} |(i_a i_b) I\rangle. \tag{A2}$$

For bosonic nuclei the sign would be opposite. The argument for determining the symmetry properties of the rest of the wave function for Hund's case (c) $\Omega=0$ states is essentially the same as for case (a) $^1\Sigma$ states, even though states in case (c) have fewer good quantum numbers than in case (a). Since Hougen's monograph [26] presents a detailed discussion of the argument for case (a), we simply adopt his phase conventions and notation and give the derivation for case (c) here.

Generally the wave function for the rotating molecule can be written as the sum of two terms, one with positive Ω and one with negative Ω. Each term is the product of an eigenfunction of the nonrotating molecular Hamiltonian and a rotational wave function, $|\Omega J\rangle$. In the special case of an $\Omega=0$ state there is no distinction between positive and negative Ω; hence the wave function for a 0_u^- state can be written simply as

$$|\psi_{mol}\rangle = |0_u^-\rangle |0J\rangle. \tag{A3}$$

The spectroscopic labels ''u'' and ''$-$'' tell how the nonrotating part of the wave function behaves under certain symmetry operations carried out in the molecule-fixed frame. In particular, the label ''u'' means that under inversion i all of the electron coordinates through the center of mass the wave function changes sign:

$$i|0_u^{\pm}\rangle = -|0_u^{\pm}\rangle. \tag{A4}$$

A $0_g^{\pm}$ state would have the opposite sign. The wave function also has a definite symmetry when the electron coordinates are reflected through a plane containing the internuclear axis (indicated by the operator σ_v):

$$\sigma_v|0_{u,g}^-\rangle = -|0_{u,g}^-\rangle. \tag{A5}$$

A $0_{u,g}^+$ state would have the opposite sign. A rotation C_2 of the electron coordinates by 180° about an axis perpendicular to this reflection plane is equivalent to inversion i followed by reflection σ_v, i.e., $C_2 = \sigma_v i$. Therefore the effect of the 180° rotation on the nonrotational 0_u^- wave function is

$$C_2|0_u^-\rangle = \sigma_v i|0_u^-\rangle = +|0_u^-\rangle. \tag{A6}$$

The effect of these symmetry operations on the rotational part of the molecular wave function is discussed by Hougen. When C_2 operates on the rotational part of an $\Omega=0$ state the result depends on whether J is odd or even:

$$C_2|0J\rangle = (-1)^J |0J\rangle. \tag{A7}$$

The effect of applying these molecule-fixed symmetry operations to $|\psi_{mol}\rangle$, including the rotational part, is equivalent to laboratory-fixed symmetry operations. In particular, applying the 180° rotation C_2 to the molecular wave function is equivalent to a lab-fixed interchange of the nuclei P. This is precisely the symmetry property we are interested in determining. Combining Eqs.(A2), (A6), and (A7) shows that the effect of a lab-fixed interchange of the nuclei on the total wavefunction for a 0_u^- state with fermionic nuclei is

$$\begin{aligned} P|\psi_{total}\rangle &= (+|0_u^-\rangle)[(-1)^J|0J\rangle][(-1)^{I+1}|(i_a i_b) I\rangle] \\ &= (-1)^{J+I+1}|\psi_{total}\rangle. \end{aligned} \tag{A8}$$

Since the total wave function must be antisymmetric under this operation, we conclude that rotational levels with even (odd) J will have even (odd) total nuclear spin I. For a 0_g^- state the right-hand side of Eq. (A4) has a plus sign. Thus for a 0_g^- state, with fermionic nuclei, rotational levels with even (odd) J have odd (even) total nuclear spin I. Since the nuclear spin does not change in an electric dipole transition this result is consistent with the general result that a $0_g^- \rightarrow 0_u^-$ transition does not have a Q branch ($\Delta J = 0$ transition).

[1] J. Weiner, V. S. Bagnato, S. Zilio, and P. S. Julienne, Rev. Mod. Phys. **71**, 1 (1999).
[2] D. J. Heinzen, in *Atomic Physics 14*, edited by D. Wineland, C. Weiman, and S. Smith (AIP Press, New York, 1995), p. 369.
[3] P. D. Lett, P. S. Julienne, and W. D. Phillips, Annu. Rev. Phys. Chem. **46**, 423 (1995).
[4] T. Walker and P. Feng, Adv. At., Mol., Opt. Phys. **34**, 125 (1994).
[5] K. M. Jones, S. Maleki, L. P. Ratliff, and P. D. Lett, J. Phys. B **30**, 289 (1997).
[6] H. Wang, X. T. Wang, P. L. Gould, and W. C. Stwalley, Phys. Rev. Lett. **78**, 4173 (1997).
[7] K. M. Jones, P. S. Julienne, P. D. Lett, W. D. Phillips, E. Tiesinga, and C. J. Williams, Europhys. Lett. **35**, 85 (1996).
[8] P. A. Molenaar, P. van der Straten, and H. G. M. Heideman, Phys. Rev. Lett. **77**, 1460 (1996).
[9] J. J. Blangé, J. M. Zijlstra, A. Amelink, X. Urbain, H. Rudolph, P. van der Straten, H. C. W. Beijerinck, and H. G. M. Heideman, Phys. Rev. Lett. **78**, 3089 (1997).
[10] L. P. Ratliff, M. E. Wagshul, P. D. Lett, S. L. Rolston, and W. D. Phillips, J. Chem. Phys. **101**, 2638 (1994).
[11] J. Weiner, F. Masnou-Seeuws, and A. Giusti-Suzor, Adv. At. Mol. Phys. **26**, 209 (1989).
[12] O. Dulieu, S. Magnier, and F. Masnou-Seeuws, Z. Phys. D: At., Mol. Clusters **32**, 229 (1994).
[13] B. Huynh, O. Dulieu, and F. Masnou-Seeuws, Phys. Rev. A **57**, 958 (1998).
[14] W. Ketterle, K. B. Davis, M. A. Joffe, A. Martin, and D. E. Pritchard, Phys. Rev. Lett. **70**, 2253 (1993).
[15] W. D. Phillips and H. J. Metcalf, Phys. Rev. Lett. **48**, 596 (1982).
[16] E. Tiesinga, C. J. Williams, P. S. Julienne, K. M. Jones, P. D. Lett, and W. D. Phillips, J. Res. Natl. Inst. Stand. Technol. **101**, 505 (1996).
[17] G. Herzberg, *Spectra of Diatomic Molecules*, 2nd ed. (Van Nostrand Reinhold, New York, 1950).
[18] M. Marinescu, Phys. Rev. A **56**, 4764 (1997).
[19] M. Movre and G. Pichler, J. Phys. B **10**, 2631 (1977).
[20] R. Heather and P. S. Julienne, Phys. Rev. A **47**, 1887 (1993).
[21] O. Dulieu, B. Levy, S. Magnier, F. Masnou-Seeuws, and Ph. Millie, Phys. Rev. Lett. **76**, 2858 (1996).
[22] A. J. Moerdijk, W. C. Stwalley, R. G. Hulet, and B. J. Verhaar, Phys. Rev. Lett. **72**, 40 (1994).
[23] A. J. Moerdijk and B. J. Verhaar, Phys. Rev. A **51**, R4333 (1995).
[24] A. Crubellier, O. Dulieu, F. Masnou-Seeuws, M. Elbs, H. Knockel, and E. Tiemann, Eur. Phys. J. D **6**, 211 (1999).
[25] M. R. Davies, J. C. Shelley, and R. J. Leroy, J. Chem. Phys. **94**, 3479 (1991).
[26] J. T. Hougen, *The Calculation of Rotational Energy Levels and Rotational Line Intensities in Diatomic Molecules*, Natl. Bur. Stand. (U.S.) Monogr. No. 115 (U.S. GPO, Washington DC, 1970).